IEEE Access
Multidisciplinary ⋮ Rapid Review ⋮ Open Access Journal

Received 2 October 2023, accepted 20 October 2023, date of publication 23 October 2023, date of current version 31 October 2023.

Digital Object Identifier 10.1109/ACCESS.2023.3327080

APPLIED RESEARCH

Direct S_{21} Calculation Using Infinitesimal Dipole Modeling

DAL-JAE YUN [1], (Member, IEEE), HOON KANG [1], IN-JUNE HWANG [2], (Member, IEEE), AND YOUNG-DAM KIM [3]

[1]Advanced Instrumentation Institute, Korea Research Institute of Standards and Science, Yuseong-gu, Daejeon 34113, Republic of Korea
[2]Division of Physical Metrology, Korea Research Institute of Standards and Science, Yuseong-gu, Daejeon 34113, Republic of Korea
[3]Department of Electronics Engineering, Chungnam National University, Daejeon 34134, Republic of Korea

Corresponding author: Young-Dam Kim (youngdamkim@cnu.ac.kr)

This work was supported in part by the Development of Core Technologies for Advanced Measuring Instruments funded by the Korea Research Institute of Standards and Science under Grant KRISS—-2023—GP2023-0012, and in part by the National Research Foundation of Korea Grant funded by the Korean Government Ministry of Education (MOE).

ABSTRACT The infinitesimal dipole modeling (IDM) technique represents the current density of the antenna under test as an array of infinitesimal dipole moments. Using the IDM concept, complicated structures of antennas and scatterers can be replaced with compact infinitesimal dipoles. With the rapid progress of antenna technology, antenna coupling analysis applicable to both near-field and far-field has become essential. The coupling phenomenon can be easily analyzed with IDM. Existing studies required additional mutual admittance calculations, and verification at the measurement level needed to be improved. In this paper, we propose an equation that directly calculates S21 from the extracted infinitesimal dipoles of the transmitter and receiver using IDM. The proposed method is demonstrated through comparison with both the numerical simulation results and measurements.

INDEX TERMS S-parameter, infinitesimal dipole modeling (IDM), source reconstruction, antenna coupling.

I. INTRODUCTION

The antenna coupling is classically a significant issue for various antenna problems such as mutual coupling of array antennas and antenna pattern distortion problems [1], wireless power transfer optimization problems [2], and optimal placement problems for maximum isolation between antennas [3], [4]. In particular, if the two antennas satisfy the far-field condition, the coupling between the two antennas can be easily and accurately analyzed through the Friis equation [5].

However, in recent antenna technology, the center frequency is increased, and the aperture of the antenna is significantly increased simultaneously [6]. In this tendency, near-field analysis must be required rather than far-field analysis. This tendency has been developed into an antenna that can form a desired radiation field by controlling the current distribution on the antenna surface, such as a metasurface [7], [8], beyond an array antenna.

If the two antennas satisfy the far-field condition, point-to-point analysis is sufficient. On the other hand, in the near-field case, volume-to-volume or surface-to-surface analysis between two antennas is required for accurate analysis of the antenna coupling. At this time, each antenna's volume or surface area can be represented by the current distribution of the antenna.

As a technique for efficiently modeling an antenna current distribution, the infinitesimal dipole modeling (IDM) technique has been mainly studied in [9], [10], [11], and [12]. A deterministic optimization algorithm can efficiently obtain antenna modeling via infinitesimal dipoles for a limited regular grid without depending on a heuristic algorithm [13]. Moreover, IDM has been verified at the measurement level for all field conditions of near-field and far-field [14], [15], [16]. A method for calculating the antenna coupling defined by S-parameters by applying the IDM technique has been

The associate editor coordinating the review of this manuscript and approving it for publication was Chan Hwang See.

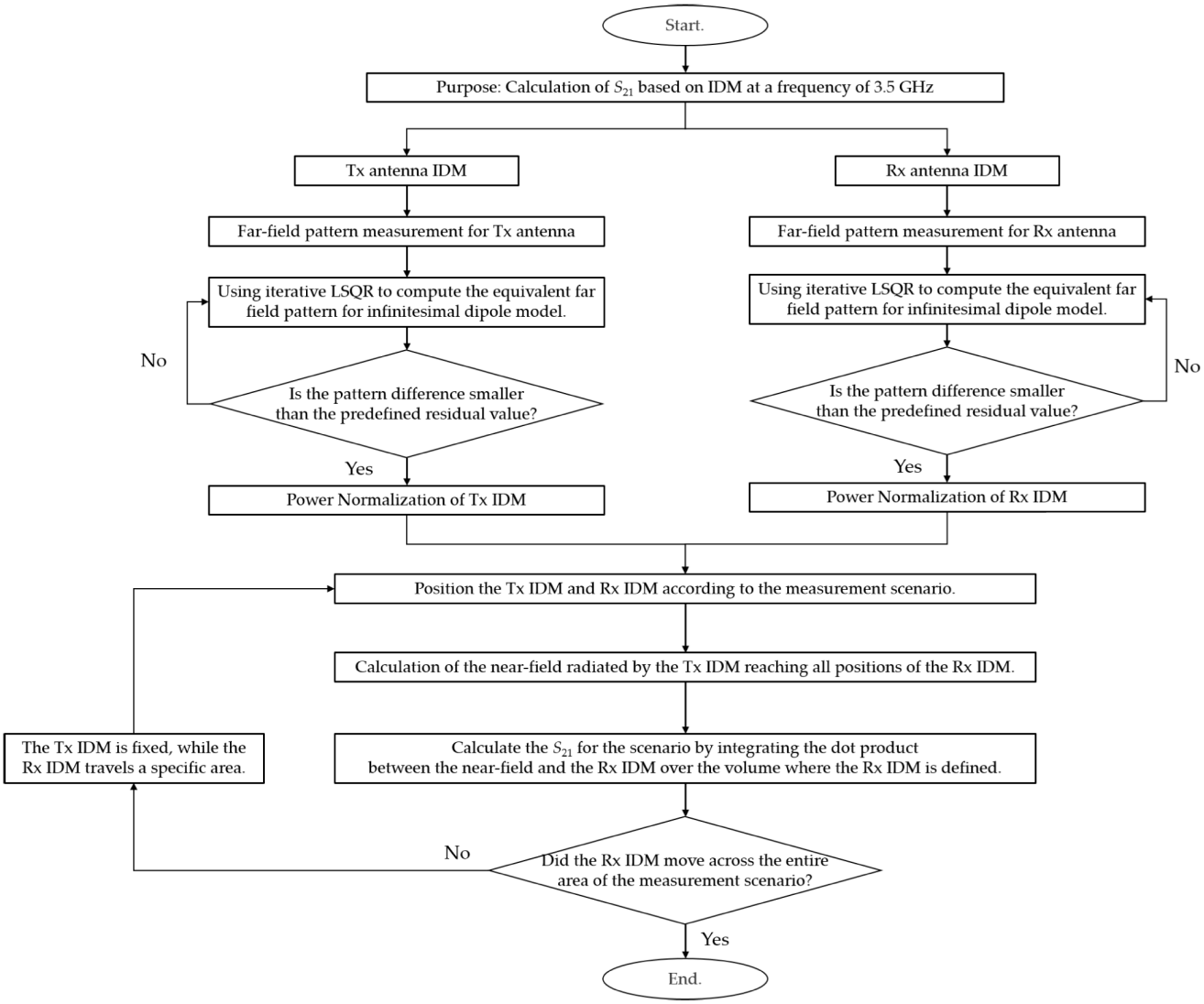

FIGURE 1. The flow chart of the proposed S_{21} calculation process using IDM.

studied in [17]. In this previous study, mutual admittance was calculated as an intermediate bridge for S_{21} calculation. Also, the calculation of S_{21} based on IDM at the measurement level needed to be verified.

In this paper, we propose an equation that directly calculates S_{21} by applying the power normalization of IDM without the calculation of mutual admittance. Additionally, the IDM-based reliability at the measurement level was verified by directly measuring the near-fields of the two antennas and estimating the results using the proposed method. The entire process of the proposed method is shown in Fig. 1. First, far-field radiation patterns of transmitting and receiving antennas are obtained. Note that the near-field pattern can also be applicable. Second, equivalent infinitesimal dipoles are extracted, identically radiating the field obtained in the previous step. Third, power normalization is required for the extracted infinitesimal dipoles [18]. Fourth, after deploying the transmitting and receiving antenna geometries modeled as infinitesimal dipoles, S_{21} is directly calculated by the proposed equation.

II. S_{21} CALCULATION OF TWO ANTENNAS VIA INFINITESIMAL DIPOLE MODELING

A. S21 FORMALISM WITH NORMALIZED CURRENT DENSITY AND IDM

As shown in Fig. 2, the energy transmission and reception of two antennas can be assumed as a two-port network system. Generally, the characteristic impedance of the antenna connected to each port may be different. Using generalized scattering parameters [19], we can define S_{21} as

$$S_{21} = \left. \frac{V_2^- \sqrt{Z_1}}{V_1^+ \sqrt{Z_2}} \right|_{V_2^+ = 0}. \tag{1}$$

where $V_1{}^+$ is an incidence voltage wave at port 1, $V_2{}^-$ is a reflected voltage wave at port 2, and Z_1 and Z_2 are the

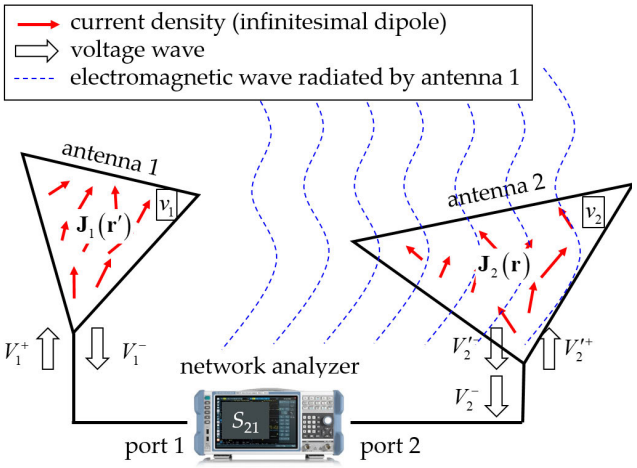

FIGURE 2. Schematic diagram of the current densities from two antennas represented by infinitesimal dipoles and S21 measurement.

characteristic impedances of port 1 and port 2, respectively. The average power P_1 delivered to antenna 1 can be described as

$$P_1 = \frac{|V_1^+|^2}{2Z_1}\left(1 - |\Gamma_1|^2\right). \tag{2}$$

where Γ_1 is a reflection coefficient at the antenna feed of port 1. The average power P_2 delivered to antenna 2 via the electromagnetic wave radiated from antenna 1 can be described as

$$P_2 = \left| \int_{v_2}\int_{v_1} \mathbf{J}_2(\mathbf{r}) \cdot \bar{\mathbf{G}}(\mathbf{r}, \mathbf{r}')\, \mathbf{J}_1(\mathbf{r}') dv_1 dv_2 \right|. \tag{3}$$

where v_1 and v_2 are the volumes of antenna 1 and antenna 2, respectively, $\mathbf{J}_1$ is the current density of antenna 1, $\mathbf{r}'$ is the position vector existing in the v_1, $\mathbf{J}_2$ is the current density of antenna 2, $\mathbf{r}$ is the position vector existing in the v_2 and $\bar{\mathbf{G}}(\mathbf{r}, \mathbf{r}')$ is a 3D free-space dyadic Green's function [18]. The physical meaning of (3) can be interpreted in three stages. In the first step, the dyadic operation of $\mathbf{J}_1$ and $\bar{\mathbf{G}}$ exhales the electric field outside of antenna 1. In the second step, the final power density is obtained through the dot product of the electric field reached by antenna 2 and $\mathbf{J}_2$. In the final step, the power density reaching antenna 2 is integrated over v_2 to obtain P_2.

Dividing both sides of (3) by $\sqrt{P_1 P_2}$, it can be expressed as

$$\sqrt{\frac{P_2}{P_1}} = \left| \int_{v_2}\int_{v_1} \hat{\mathbf{J}}_2(\mathbf{r}) \cdot \bar{\mathbf{G}}(\mathbf{r}, \mathbf{r}')\, \hat{\mathbf{J}}_1(\mathbf{r}') dv_1 dv_2 \right|. \tag{4}$$

where $\hat{\mathbf{J}}_1$ and $\hat{\mathbf{J}}_2$ respectively are normalized current density of antenna 1 and antenna 2. The power normalization can be defined as

$$\hat{\mathbf{J}}_n = \left. \frac{\mathbf{J}_n}{\sqrt{P_n}} \right|_{n=1,2}. \tag{5}$$

At the boundary of the transmission line connected to antenna 2, the three voltage waves can be represented as $V_2'^-$, $V_2'^+$, and V_2^-. Assume that the reflection coefficient due to the mismatch between the impedance of antenna 2 and the transmission line is Γ_2. The relation between $V_2'^-$ and $V_2'^+$ is represented as $V_2'^+ = \Gamma_2 V_2'^-$. The average power of port 2 can be expressed as (6) by removing the reflected energy from the power P_2.

$$\frac{|V_2^-|^2}{2Z_2} = P_2\left(1 - |\Gamma_2|^2\right). \tag{6}$$

When combining (2), (4), and (6), the relation between V_2^- and V_1^+ can be derived as

$$\frac{|V_2^-|^2}{2Z_2} = \left| \int_{v_2}\int_{v_1} \hat{\mathbf{J}}_2(\mathbf{r}) \cdot \bar{\mathbf{G}}(\mathbf{r}, \mathbf{r}')\, \hat{\mathbf{J}}_1(\mathbf{r}') dv_1 dv_2 \right|^2 \times \frac{|V_1^+|^2}{2Z_1}\left(1 - |\Gamma_1|^2\right)\left(1 - |\Gamma_2|^2\right). \tag{7}$$

The final goal is to formulate S_{21} using the normalized current densities $\hat{\mathbf{J}}_1$ and $\hat{\mathbf{J}}_2$. (7) can be converted regarding the form of (1). Finally, $|S_{21}|^2$ can be represented as

$$|S_{21}|^2 = \left| \int_{v_2}\int_{v_1} \hat{\mathbf{J}}_2(\mathbf{r}) \cdot \bar{\mathbf{G}}(\mathbf{r}, \mathbf{r}')\, \hat{\mathbf{J}}_1(\mathbf{r}') dv_1 dv_2 \right|^2 \times \left(1 - |\Gamma_1|^2\right)\left(1 - |\Gamma_2|^2\right). \tag{8}$$

(8) provides only the amplitude information of S_{21}. The phase of S_{21} is also an essential factor, and it has the meaning of time delay corresponding to the physical location difference between antenna 1 and antenna 2. We define angle(•) as a function that returns the phase of any complex number. Therefore, the phase of S_{21} can be obtained by

$$\text{angle}\,(S_{21}) = \text{angle}\left(\int_{v_2}\int_{v_1} \hat{\mathbf{J}}_2(\mathbf{r}) \cdot \bar{\mathbf{G}}(\mathbf{r}, \mathbf{r}')\, \hat{\mathbf{J}}_1(\mathbf{r}') dv_1 dv_2 \right). \tag{9}$$

In Fig. 2, the two antennas are modeled as electric current densities $\mathbf{J}_1$ and $\mathbf{J}_2$ through the IDM process [9]. In order to obtain individual IDM results of two antennas, we already know the simulation or measurement results when antenna 1 and antenna 2 exist alone. Moreover, suppose the two antennas are not very close to each other within one wavelength. The logical justification for the formula being valid at antenna distances of more than one wavelength is detailed in [17]. Essentially, the dyadic Green's function has the distance difference between the source point $\mathbf{r}'$ and the observation point $\mathbf{r}$ in its denominator. For very short distances relative to the wavelength, one can assume numerically that the denominator approaches zero, leading to diverging errors in numerical analysis. To address this issue, [17] conducted experiments by varying the distance between the two antennas, and it provides satisfactory accuracy even at 0.5 wavelengths. In that

TABLE 1. Qualitative Comparison of Research from The Perspective of S_{21} Calculation.

Reference. (Year)	IDM Optimization Variables	IDM Optimization Method	Mutual Admittance Calculation	Power Normalization	Computational Complexity for S_{21} Calculation
[9] (2007)	7 position (3) + complex coefficients (2) + orientation direction (2)	QPSO*	O	X	medium
[17] (2019)	3 complex coefficients for x, y, z direction	LSQR	O	X	low
[4] (2022)	use current distribution obtained by full-wave simulation		O	X	very high (require full-wave simulation)
This Paper (2023)	3 complex coefficients for x, y, z direction	LSQR	X	O	very low (direct S_{21} calculation)

QPSO*: Quantum Particle Swarm Optimization

case, Γ_1 and Γ_2 can also be assumed to be the results obtained by simulation or measurement of a single antenna used in IDM.

This paper aims to calculate S_{21} when two independently known antennas are arranged in an arbitrary shape. Mathematically, IDM expresses the actual current density function as a sampling and series sum of delta functions on a grid within a specific antenna volume [13]. Therefore, the continuous integral of (8) and (9) is changed to a series sum, and its calculation can be done very rapidly and efficiently.

B. POWER NORMALIZATION OF CURRENT DENSITY

The electric field on the observation position vector $\mathbf{r}$ emitted by the current density on $\mathbf{r}'$ is represented as

$$\mathbf{E}(\mathbf{r}) = \int_v \bar{\mathbf{G}}(\mathbf{r}, \mathbf{r}') \mathbf{J}(\mathbf{r}') \, dv. \tag{10}$$

where $\mathbf{r}'$ only exists inside the antenna volume v, and $\mathbf{r}$ is outside the antenna. Suppose $|\mathbf{r} - \mathbf{r}'|$ is so large compared to the antenna diameter that the far-field assumption can be valid. With the far-field assumption, $\mathbf{r}$ can be converted to the observation angle θ and ϕ in spherical coordinates. By integrating the diverging power flux density over the closed Gaussian sphere surface, the total power emitted by the antenna can be measured as

$$P = \int_0^{2\pi} \int_0^{\pi} \frac{|\mathbf{E}(\theta, \phi)|^2}{2\eta} r^2 \sin\theta d\theta d\phi. \tag{11}$$

where η is a characteristic impedance of a homogeneous medium in which electromagnetic wave is radiated, and r is the distance from the origin to the observation point located in the far-field.

In summary, power normalization of the current density can be obtained by dividing by the square root of the total emitted power via (11). Normalization can be performed as in (5) for both transmitting and receiving modes by antenna reciprocity [18]. Using the reciprocity theorem is consistent across all conventional methods [4], [9], [17], and the proposed method. In this paper, we particularly emphasize the power normalization of the current density as a novelty point. This is well illustrated in Table 1. Calculating mutual admittance requires additional separate calculations, and typically the self-impedance of the antenna is required. On the other hand, the proposed method allows for immediate calculation without the requirement for mutual admittance calculations, based on the power normalization technique. Especially, for the self-impedance part of the conventional research, one can simply use the generally known S_{11} value of a typical antenna. This suggests that S_{21} can be calculated using only the far-field radiation characteristics of the antennas.

III. VALIDATION RESULTS

A. IDM FOR TRANSMITTING AND RECEIVING ANTENNAS

To validate the proposed method, infinitesimal dipoles of each transmitting and receiving antenna are first extracted. The transmitting antenna is a double-ridged broadband horn from Fei Teng Wireless Technologies (model HA-0218G-NF [20]). The frequency range of the horn is from 2 GHz to 18 GHz for a 2:1 voltage standing wave ratio (VSWR). The receiving antenna is an open-ended waveguide from NSI-MI Technologies (model ANT-WGP-2.6-3.95 [21]). This rectangular probe conforms to the WR-284 format and has a frequency range of 2.60 GHz to 3.95 GHz for a 2.5:1 VSWR.

Computer-aided design (CAD) models of the antennas were constructed based on the specifications in the datasheet, as shown in Fig. 3(a) and Fig. 4(a).

When calculating S_{21}, transmitting and receiving antennas have orientations facing each other. The direction of the receiving probe is thus reversed. Three-dimensional (3-D) radiation patterns were calculated using the method of moments (MoM), shown in Fig. 3(b) and Fig. 4(b). The 3-D far-field patterns are obtained at intervals of 3 degrees in both the azimuth and elevation directions. Here, the MoM results are computed with the MATLAB antenna toolbox, and the center frequency is 3.5 GHz. Infinitesimal dipoles of each antenna were then extracted using the IDM process [17]. Fig. 3(c) and Fig. 4(c) show power normalized current density

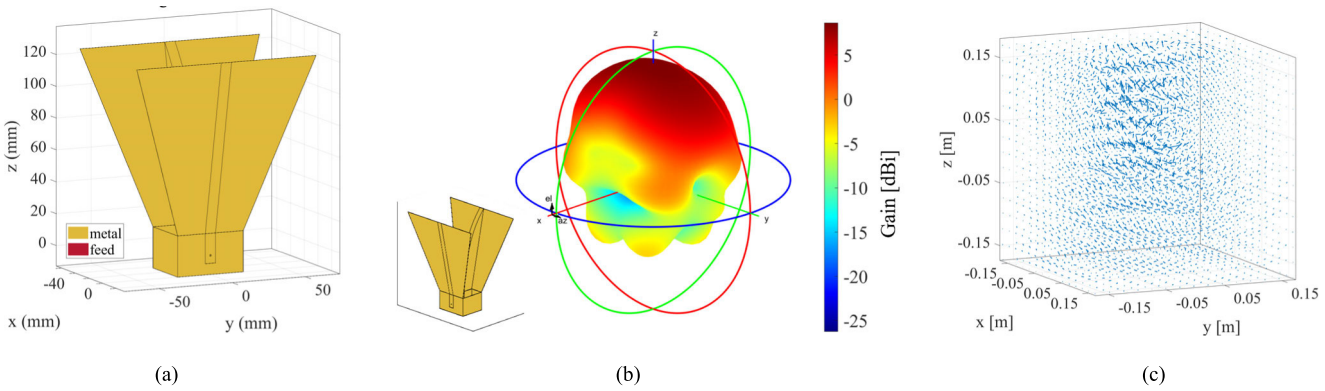

FIGURE 3. Transmitting ridged horn antenna (a) geometry (b) 3-D far-field radiation pattern (c) equivalent infinitesimal dipole model.

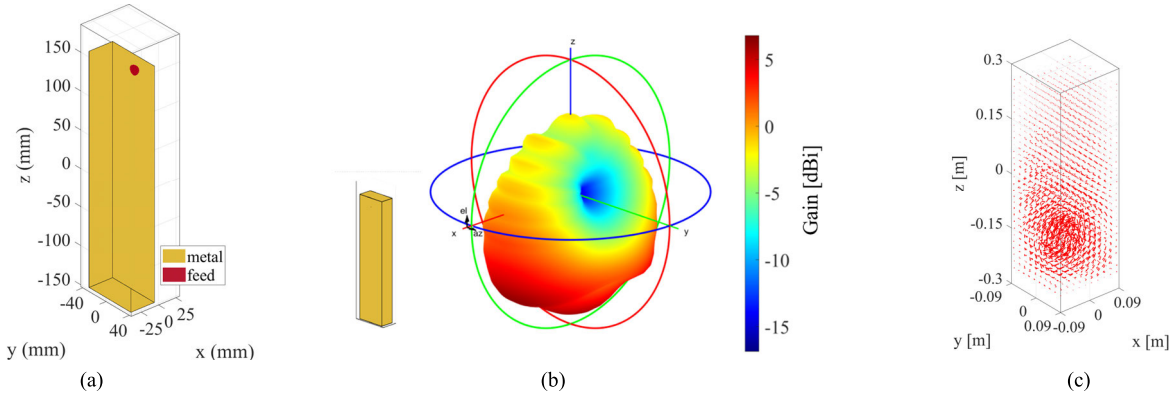

FIGURE 4. Open-ended waveguide probe (a) geometry (b) 3-D far-field radiation pattern (c) equivalent infinitesimal dipole model.

distributions. The transmitting horn is modeled as a regular grid of infinitesimal dipoles of 15 × 15 × 35 in a 4λ cube. The validation of the accurate extraction of the IDM can be ascertained by re-radiating the extracted IDMs from Fig. 3(c) and Fig. 4(c) using (10). We can assess whether Fig. 3(b) and Fig. 4(b) can be precisely reconstructed. The quantitative accuracy of this process is defined by the residual error of the LSQR.

The modeling accuracy in IDM process is quantified by the relative residual error in LSQR solver of MATLAB. LSQR is an algorithm for sparse linear equations and sparse least squares [25]. The IDM accuracy of the transmitting horn is –25.2 dB. The receiving probe is modeled as a regular grid of infinitesimal dipoles of 10 × 10 × 30 in a cuboid of 2λ width, 2λ length, and 6λ height. The IDM accuracy of the receiving probe is –22.9 dB.

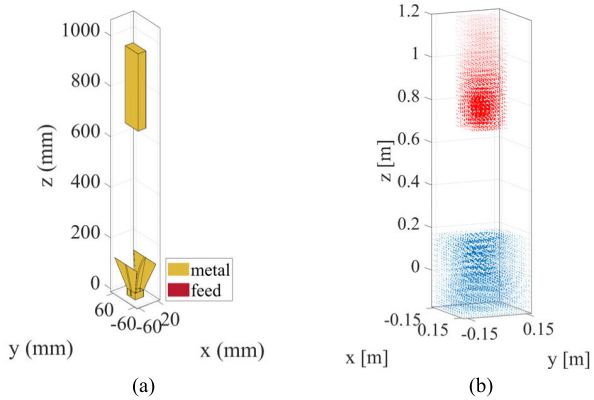

FIGURE 5. Geometrical configurations of the S21 acquisition (aligned with respect to the two antenna apertures) (a) for full-wave simulation (b) for IDM-based calculation.

B. VALIDATION FROM NUMERICAL SIMULATIONS

To demonstrate the accuracy of the proposed method, we compared S_{21} calculation results with the numerical simulation results. Configurations of the S_{21} calculations using the full-wave simulation and proposed method are shown in Fig. 5(a) and Fig. 5(b), respectively. The distance between the aperture of the transmitting horn and the aperture of the receiving probe was set at 535 mm. In Fig. 5(a), the receiving probe moved in quarter-wavelength intervals from –1.4 m to 1.4 m in both x- and y-axis directions. The S_{21} simulation result as a function of spatial movement of the receiver is thus a matrix of 131 × 131 size. In a similar way, by translational movement of the infinitesimal dipoles equivalent to the receiving probe at quarter-wavelength intervals, the S_{21} calculation result was obtained, as shown in Fig. 5(b).

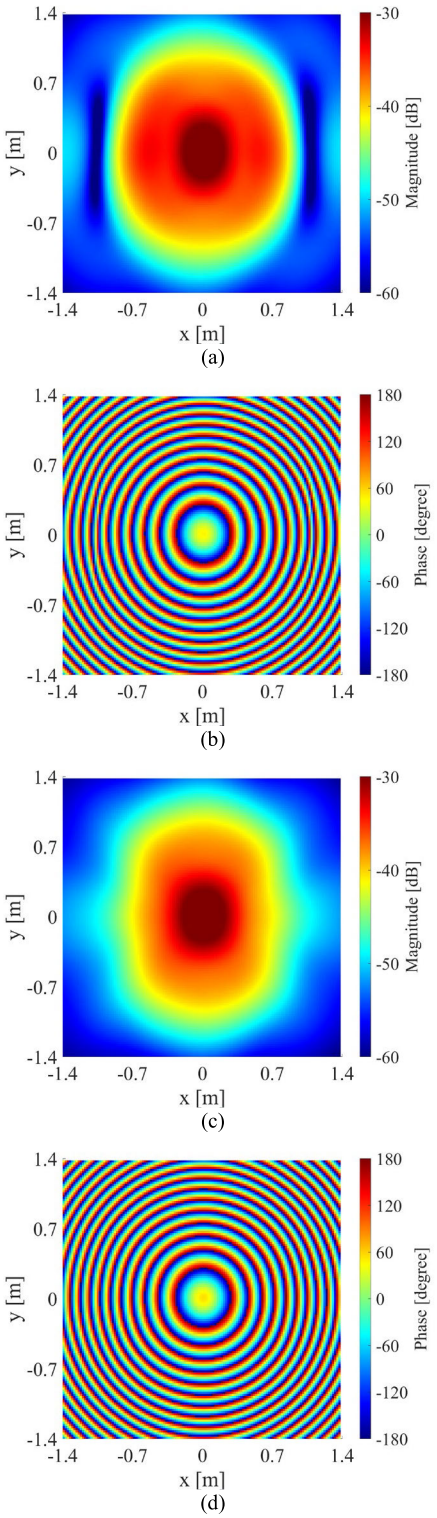

FIGURE 6. Results corresponding to Fig. 5 (a) magnitude result of the full-wave simulation (b) phase result of the full-wave simulation (c) magnitude result of the proposed method (d) phase result of the proposed method.

Fig. 6 shows comparisons of S_{21} results. Magnitudes of S_{21} for full-wave simulation and the proposed method are presented in Fig. 6(a) and Fig. 6(c), respectively. Phases of S_{21} for full-wave simulation and the proposed method are presented in Fig. 6(b) and Fig. 6(d), respectively. Both magnitude and phase results are analogous.

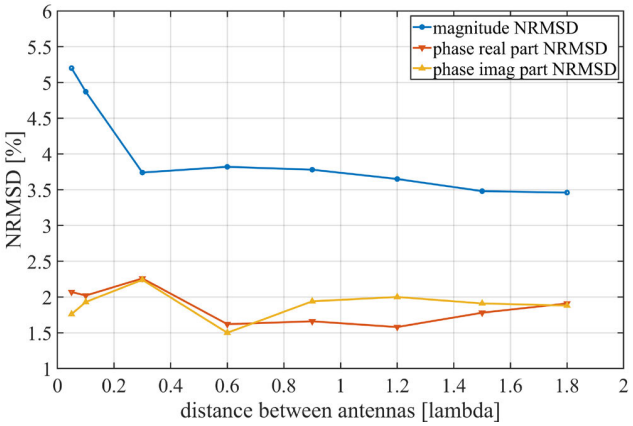

FIGURE 7. Comparison of the error in the proposed method depending on the distance between antennas.

To quantify the difference between the two images, we introduce the normalized root-mean-square deviation (NRMSD) concept as (12). The above measure of accuracy quantifies the error of the proposed method by aggregating the difference in intensity between two images.

$$NRMSD = \frac{1}{O_{1,\max} - O_{1,\min}} \sqrt{\frac{\sum_{h=1}^{H} \sum_{w=1}^{W} (O_{1,h,w} - O_{2,h,w})^2}{HW}} \tag{12}$$

where O_1 and O_2 are the intensities of the reference and predicted images, respectively. H and W denote the height and width of the image, respectively.

We analyzed the magnitude and phase of the full-wave simulation and the proposed technique using NRMSD. The linear scale NRMSD is represented as 4.73% for the magnitude. To analyze the NRMSD for the phase, the phase was complexified and the NRMSD of the real and imaginary terms were compared. The NRMSD is 2.09% for the real term and 2.07% for the imaginary term. Specifically, for the magnitude, the maximum value of the reference result is –27.15 dB at the position (0.01, –0.01), while the proposed technique shows a maximum value of –27.16 dB at the position (0.01, –0.01). Therefore, it can be observed that the proposed method effectively emulates the reference result.

We conducted an additional demonstration regarding the accuracy of the proposed method. We performed both the full-wave simulation and the proposed method by varying the distance between the horn antenna and the waveguide from 0.05λ to 1.8λ. Fig. 7 depicts the accuracy results of the two techniques using NRMSD. As the distance between the two antennas becomes closer, the error increases. The reason is that when performing the IDM, the influence of the other antenna is not taken into consideration. In the full-wave

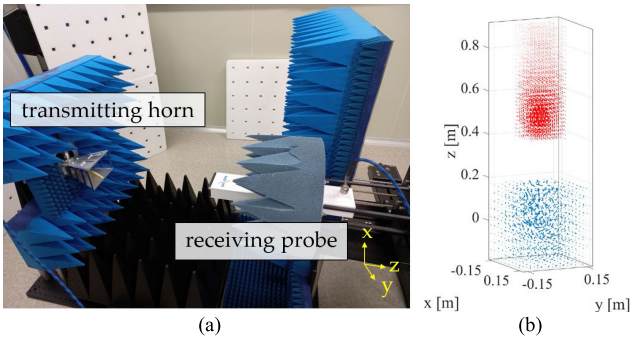

FIGURE 8. Geometrical configurations of the S21 acquisition (aligned with respect to the two antenna apertures) (a) for measurement (b) for IDM-based calculation.

simulation, the mutual coupling between the two antennas is considered, resulting in more accurate results. In other words, as the distance becomes closer, the denominator of Green's function in our proposed method diverges, causing a decline in accuracy. Therefore, we can trust the proposed technique starting from a spacing of about 0.3λ.

C. VALIDATION FROM MEASUREMENTS

To validate the feasibility of the proposed method, we further compared S_{21} calculation results with the measurements. The center frequency was set to 3.5 GHz. Configurations of the measurement system and the proposed method are shown in Fig. 8(a) and Fig. 8(b), respectively. Pyramidal electromagnetic absorbers from RIKEN environmental system and Siepel were deployed around the measurement system to minimize electromagnetic scattering on the walls and floors. The receiving probe was attached to a 3-axis stage and moved translationally. The vector network analyzer (VNA) used for the measurement is from Rhode Schwarz (model R&SZNA43 [22]). The operational frequency range of the VNA is from 10.0 MHz to 43.5 GHz. The dynamic range of the VNA is up to 146 dB.

The aperture-to-aperture distance between the transmitter and receiver was set to 265 mm. In Fig. 8(a), the receiving probe translationally moved in 10 mm from –150 mm to 150 mm in both x- and y-axis directions. Note that the travel range of the stage (model LTS300 from Thorlabs) is 300 mm. Therefore, the S_{21} measurement results as a function of spatial movement of the receiver is thus a matrix of 31 × 31 size. An in-house program was developed to automate hundreds of measurements. First, translational movement of the receiver was implemented at intervals of 10 mm using the software development kit (SDK) of the stage. Since the repeatability and accuracy of the stage are a few micrometers, the effect of positional uncertainty is negligible in the measurement. When the receiving probe arrives at the desired position, S_{21} measurement results from the VNA are automatically stored using standard commands for programmable instruments (SCPI). From the IDM point of view, the S_{21} matrix can also be calculated by performing translational movement

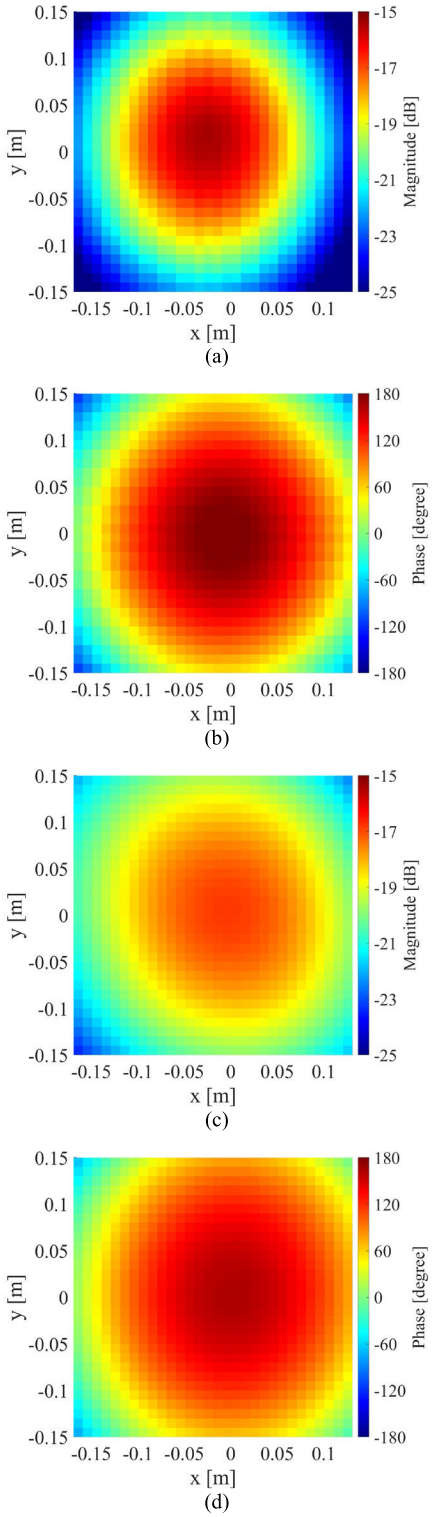

FIGURE 9. Results corresponding to Fig. 8(a) magnitude result of the measurement (b) phase result of the measurement (c) magnitude result of the proposed method (d) phase result of the proposed method.

of infinitesimal dipoles equivalent to the receiving probes at equal intervals, as shown in Fig. 8(b).

The measured S_{21} magnitude and phase surface map are shown in Fig. 9(a) and Fig. 9(b), respectively. And the

estimated S_{21} magnitude and phase surface map are shown in Fig. 9(c) and Fig. 9(d), respectively. We quantified the magnitude and phase results of the measurements and the proposed method. The linear scale NRMSD is represented as 15.63% for the magnitude. Regarding the accuracy of the phase, the NRMSD for the real term is 2.53%, while the NRMSD for the imaginary term is 2.71%. Specifically, for the magnitude, the maximum value of the measurement result is –15.38 dB at the position (0.01, –0.01), while the proposed method shows a maximum value of –16.81 dB at the position (0.01, 0). The proposed method calculates accurate S_{21} phase results in comparison with the measurement, as shown in Fig. 9. However, it can be seen that the magnitude differs slightly at lower magnitude levels. The reason for the discrepancy is the influence that arises in relation to the measurement. First, there may be an effect due to geometrical tolerances such as antenna orientation deviation during the installation and assembly of the measurement system. Second, although the system is covered with absorbers, a slight change in the antenna pattern may occur due to an external environment. Third, it is due to magnitude loss from devices such as cables and antenna connectors, etc. Therefore, the installed measurement system can minimize the effects of environmental or human intervention during operation by automating most tasks with SCPI. However, issues like electromagnetic scattering due to the presence of the operator and installation errors resulting from humans directly installing the transmitters and receivers can still occur. To address these errors, from an implementation perspective, there are methods like using optical solutions such as lasers to guide installations, and the time gating method of VNA can be used to minimize the effects of scatterers. Subsequent research is required to strengthen the proposed theory by considering the aforementioned effect from the environment and humans as specific factors.

In the far-field region, various asymptotic methods, such as the Friis equation and ray tracing, are employed to efficiently and accurately analyze the coupling between antennas. However, in the near field, accurately deriving the S_{21} value of antenna coupling coefficients without full-wave simulation presents a challenge. This study presents a technique to conveniently estimate the S_{21} coupling coefficient between two antennas in the near field. The S_{21} value between the two antennas can be approximated using the channel coefficient between them, facilitating the analysis of communication performance metrics, such as capacity and degrees of freedom. Especially, this approach has potential applications in the channel analysis of massive MIMO and orbital angular momentum (OAM) wave communications [23], [24], particularly when utilizing large apertures like metasurfaces and uniform circular arrays (UCA).

IV. CONCLUSION

This paper proposes calculating the energy transfer efficiency between two antennas regardless of the near-field and far-field of the antennas. Specifically, S_{21} is directly calculated using power normalized IDMs of individual antennas without full-wave simulations of the entire antenna system. Therefore, S_{21} can be efficiently calculated for various geometrical configurations of the two antennas. The IDM-based reliability at the measurement level was verified by directly measuring the near fields of the two antennas and estimating the results using the proposed method.

Since these infinitesimal dipoles represent the current distribution of the antenna, they can be easily applied to the analysis of OAM waves and metasurface antennas that transmit radio waves by controlling the antenna current distribution on a large surface. Furthermore, by constructing the proposed method inversely, IDM can be performed from the measured S_{21}. The far- and near-fields of the antenna under test can then be estimated from the IDM obtained above. Our research team is conducting follow-up research on this subject.

REFERENCES

[1] W. C. Gibson, *The Method of Moments in Electromagnetics*. Boca Raton, FL, USA: CRC Press, 2007.

[2] P. Nepa and A. Buffi, "Near-field-focused microwave antennas: Near-field shaping and implementation," *IEEE Antennas Propag. Mag.*, vol. 59, no. 3, pp. 42–53, Jun. 2017.

[3] D. Su, Z. Yang, and Q. Wu, "Characteristic mode assisted placement of antennas for the isolation enhancement," *IEEE Antennas Wireless Propag. Lett.*, vol. 17, no. 2, pp. 251–254, Feb. 2018.

[4] M. A. Jamshed, T. W. C. Brown, and F. Héliot, "Dual antenna coupling manipulation for low SAR smartphone terminals in talk position," *IEEE Trans. Antennas Propag.*, vol. 70, no. 6, pp. 4299–4306, Jun. 2022.

[5] C. A. Balanis, *Antenna Theory: Analysis and Design*. Hoboken, NJ, USA: Wiley, 2016.

[6] W. Hong, Z. H. Jiang, C. Yu, J. Zhou, P. Chen, Z. Yu, H. Zhang, B. Yang, X. Pang, M. Jiang, Y. Cheng, M. K. T. Al-Nuaimi, Y. Zhang, J. Chen, and S. He, "Multibeam antenna technologies for 5G wireless communications," *IEEE Trans. Antennas Propag.*, vol. 65, no. 12, pp. 6231–6249, Dec. 2017.

[7] S. Maci, G. Minatti, M. Casaletti, and M. Bosiljevac, "Metasurfing: Addressing waves on impenetrable metasurfaces," *IEEE Antennas Wireless Propag. Lett.*, vol. 10, pp. 1499–1502, 2011.

[8] D. González-Ovejero, G. Minatti, G. Chattopadhyay, and S. Maci, "Multibeam by metasurface antennas," *IEEE Trans. Antennas Propag.*, vol. 65, no. 6, pp. 2923–2930, Jun. 2017.

[9] S. M. Mikki and A. A. Kishk, "Theory and applications of infinitesimal dipole models for computational electromagnetics," *IEEE Trans. Antennas Propag.*, vol. 55, no. 5, pp. 1325–1337, May 2007.

[10] S. M. Mikki and Y. M. M. Antar, "Near-field analysis of electromagnetic interactions in antenna arrays through equivalent dipole models," *IEEE Trans. Antennas Propag.*, vol. 60, no. 3, pp. 1381–1389, Mar. 2012.

[11] S. Clauzier, S. M. Mikki, and Y. M. M. Antar, "Design of near-field synthesis arrays through global optimization," *IEEE Trans. Antennas Propag.*, vol. 63, no. 1, pp. 151–165, Jan. 2015.

[12] S. Clauzier, S. M. Mikki, and Y. M. M. Antar, "A generalized methodology for obtaining antenna array surface current distributions with optimum cross-correlation performance for MIMO and spatial diversity applications," *IEEE Antennas Wireless Propag. Lett.*, vol. 14, pp. 1451–1454, 2015.

[13] S. J. Yang, Y. D. Kim, D. J. Yun, D. W. Yi, and N. H. Myung, "Antenna modeling using sparse infinitesimal dipoles based on recursive convex optimization," *IEEE Antennas Wireless Propag. Lett.*, vol. 17, no. 4, pp. 662–665, Apr. 2018.

[14] S.-J. Yang, Y.-D. Kim, H.-W. Jo, and N.-H. Myung, "Alternative method for obtaining antenna current Green's function based on infinitesimal dipole modeling," *IEEE Trans. Antennas Propag.*, vol. 67, no. 4, pp. 2583–2590, Apr. 2019.

[15] J.-I. Oh, S. J. Yang, S. Kim, J.-W. Yu, and Y. D. Kim, "Antenna diagnostics based on infinitesimal dipole modeling with limited measurement on antenna aperture," *IEEE Antennas Wireless Propag. Lett.*, vol. 21, no. 5, pp. 923–927, May 2022.
[16] J.-H. Han, W. Lee, and Y. D. Kim, "Infinitesimal dipole modeling from sparse far-field patterns for predicting electromagnetic characteristics of unknown antennas," *IEEE Trans. Antennas Propag.*, vol. 70, no. 11, pp. 10245–10252, Nov. 2022.
[17] Y.-D. Kim, S.-J. Yang, Y.-S. Kang, I.-J. Hwang, and J.-W. Yu, "Mutual admittance of two arbitrary antennas in nonplanar skew positions based on infinitesimal dipole modeling," *IEEE Trans. Antennas Propag.*, vol. 67, no. 11, pp. 6705–6713, Nov. 2019.
[18] J. Knapp, "Antenna field measurements and transformations in arbitrary echoic environments," Ph.D. dissertation, Dept. Elect. Eng., Tech. Univ. Munich, Munich, Germany, 2021.
[19] D. M. Pozar, *Microwave Engineering*. New York, NY, USA: Wiley, 2005.
[20] FT-RF. (Feb. 2023). *2 GHz to 18 GHz Double Ridged Broadband Waveguide Horn Antenna*. [Online]. Available: https://horn.ft-RF.com.tw/2ghz-to-18ghz-double-ridged-broadband-waveguide-horn-antenna/
[21] NSI-MI. (Feb. 2023). *Waveguide Probes*. [Online]. Available: https://www.nsi-mi.com/products/antenna-products/wabeguide-probes/
[22] R. Schwarz. (Feb. 2023). *R&S ZNA43*. [Online]. Available: https://www.rohde-schwarz.com/kr/products/test-and-measurement/network-analyzers/rs-zna-vector-network-analyzers_63493-551810.html
[23] S. Kiani, P. Rezaei, and M. Fakhr, "On-chip coronavirus shape antenna for wide band applications in terahertz band," *J. Opt.*, vol. 52, no. 2, pp. 860–867, Jan. 2023.
[24] P. Sohrabi, P. Rezaei, S. Kiani, and M. Fakhr, "A symmetrical SIW-based leaky-wave antenna with continuous beam scanning from backward-to-forward through broadside," *Wireless Netw.*, vol. 27, no. 8, pp. 5417–5424, Nov. 2021.
[25] C. C. Paige and M. A. Saunders, "LSQR: An algorithm for sparse linear equations and sparse least squares," *ACM Trans. Math. Softw.*, vol. 8, no. 1, pp. 43–71, Mar. 1982.

DAL-JAE YUN (Member, IEEE) received the B.S. degree in electrical engineering from Hanyang University, Seoul, South Korea, in 2012, and the Ph.D. degree in electrical engineering from KAIST, Daejeon, South Korea, in 2018. He is currently a Senior Researcher with the Korea Research Institute of Standards and Science (KRISS). His current research interests include electromagnetic scattering analysis and inverse synthetic aperture radar imaging algorithms.

HOON KANG received the B.S. degree in mechanical engineering and the M.S. degree in mechatronics engineering from Korea Maritime University, Busan, South Korea, in 2011 and 2013, respectively. He was a Researcher with the Korea Institute of Industrial Technology (KITECH), Daegu, South Korea, from 2014 to 2017. He is currently a Senior Engineer with the Advanced Instrumentation Institute, Korea Research Institute of Standards and Science (KRISS), Daejeon, South Korea. His current research interests include the design, control, and evaluation of scientific instruments.

IN-JUNE HWANG (Member, IEEE) received the B.S. degree in electrical and electronic engineering from Yonsei University, Seoul, Republic of Korea, in 2013, and the M.S. and Ph.D. degrees in electrical engineering from the Korea Advanced Institute of Science and Technology (KAIST), Daejeon, Republic of Korea, in 2015 and 2019, respectively.

Since 2019, he has been a Senior Research Scientist with the Division of Physical Metrology, Electromagnetic Wave Metrology Group, Korea Research Institute of Standards and Science (KRISS), Daejeon. His current research interests include electromagnetic field strength, antenna measurement standards, millimeter-wave antennas, phased array antenna systems, energy harvesting, and RF wireless power transfer.

YOUNG-DAM KIM was born in Suwon, South Korea, in 1988. He received the B.S. degree in electronics engineering from Ajou University, Suwon, in 2011, and the M.S. and Ph.D. degrees in electrical engineering from the Korea Advanced Institute of Science and Technology (KAIST), Daejeon, South Korea, in 2013 and 2017, respectively. He was a Senior Engineer with Samsung Electronics Network Business, Suwon, in 2017. He was a Postdoctoral Researcher with KAIST, in 2018. He was a Senior Researcher with the Agency for Defense Development (ADD), South Korea, from 2019 to 2020. He is currently an Assistant Professor with the Department of Electronics Engineering, Chungnam National University (CNU), Daejeon. His current research interests include the analysis of active phased antenna arrays and electromagnetic scattering problems based on applied computational electromagnetics.